17th World Conference on Earthquake Engineering, 17WCEE
Sendai, Japan - September 13th to 18th 2020

OPTIMAL GAIN CALIBRATION OF ADAPTIVE MODEL-BASED COMPENSATION FOR REAL-TIME HYBRID SIMULATION TESTING

G. Fermandois[(1)], C. Galmez[(2)], M. Valdebenito[(3)]

[(1)] *Assistant Profesor, Departamento de Obras Civiles – Universidad Técnica Federico Santa María, Santiago, Chile, gaston.fermandois@usm.cl*
[(2)] *M.S. Student, Departamento de Obras Civiles – Universidad Técnica Federico Santa María, Santiago, Chile, cristobal.galmez.12@sansano.usm.cl*
[(3)] *Associate Profesor, Departamento de Obras Civiles – Universidad Técnica Federico Santa María, Valparaíso, Chile, marcos.valdebenito@usm.cl*

Abstract

Real-time hybrid simulation (*RTHS*) is an experimental technique for structural testing, where a critical element is studied in the laboratory, and the rest of the structure is represented through numerical simulations. The boundary conditions on the physical specimen are imposed by a transfer system (i.e., actuators), and it is essential to minimize synchronization errors between numerical and experimental subdomains to ensure not only accurate but stable results during the experiment. Many control methods have been proposed to compensate actuator dynamics and minimize synchronization errors. However, current methods require either manual tuning of controller parameters, which is a time-consuming and challenging process. Alternatively, model-based approaches require good knowledge of the transfer system (i.e., a calibrated model through system identification), including any dynamic interactions with the physical specimen and surrounding loading equipment. Thus, additional costs and sometimes premature damage to the physical specimen are expected during the controller calibrations.

This paper conducts a detailed study on adaptive compensation for *RTHS*, with a focus on robustness against the choice of adaptive gains. The main goal is to design a dynamic compensator that does not require previous knowledge of the specimen interaction with the transfer system. Hence, an adaptive gain optimization procedure is proposed to improve the robustness of this technique. Optimal adaptive gains are obtained through a particle swarm optimization approach, where the evaluation of the objective function is carried out by a series of numerical simulations of the interactions between specimen-transfer systems. As a proof-of-concept, this method is evaluated using virtual *RTHS* simulations, including the controller design and calibration processes. The method achieves excellent compensation using the same controller for various experimental scenarios, including different partitioning cases, uncertainties in the actuator and experimental substructure parameters, and noise in measured signals. Through this development, structural laboratories will be capable of testing different substructures while avoiding unnecessary system identification to capture specimen interaction, and without a significant compromise in accuracy or laboratory safety.

Keywords: Real-time hybrid simulation; dynamic compensation; adaptive control; adaptive gain calibration; particle swarm optimization.

1. Introduction

Laboratory tests are essential to study the behavior of structural systems and materials subjected to dynamic loadings, such as those produced by earthquakes. Experimental techniques such as cyclic tests and shake table tests are quite ubiquitous in structural engineering. Another technique called real-time hybrid simulation (*RTHS*) has proven as a cost-effective and realistic approach to conducting seismic performance assessment, taking full advantage of available equipment installed in laboratories (e.g., dynamic actuators or shake tables).

Real-time hybrid simulation (*RTHS*) is an experimental technique for structural testing. A critical element is studied in the laboratory, while the rest of the structure is represented through numerical simulations [1,2]. At each time step, the calculated displacements are imposed on the experimental substructure by a transfer system (i.e., actuators). Then, the restitutive forces are measured and incorporated into the equations of motion to calculate the displacement at the following time step. Representing numerically part of the structure reduces the costs and requirements of the laboratory, while the experimental part results in a realistic analysis of the physical specimen.

A crucial aspect of *RTHS* tests is the correct application of the boundary conditions on the experimental substructure. The dynamic properties of the transfer system and their interaction with the experimental substructure produces synchronization errors (amplitude or delay errors) between commanded and measured displacements [3]. The most harmful error is the delay between the physical and numerical domain. When this is introduced in the equation of motion, it can cause not only precision problems but also instability [4]. Thus, different methods have been proposed to compensate for the dynamic of the transfer system and thus minimize synchronization errors. Early methods reported in the literature are based on polynomial extrapolation, assuming a constant delay [5]. Other methods are based on representing the system to be controlled with a first-order transfer function and applying the inverse of this function to compensate for the dynamic of the actuator [6]. More sophisticated methods are known as model-based compensation, where the controller is designed based on a higher-order estimate of the transfer function of the plant [7]. Model-based compensation has excellent results if a good plant model is available to design the controller. However, there are no guarantees of accuracy or stability when there is significant uncertainty on the model.

Adaptive compensation has been proposed in *RTHS* testing to provide excellent controller performance when there is uncertainty or significant non-linearity in the control plant. Some adaptive methods consist of compensation through a first-order transfer function, where parameters of the function are adjusted during the test based on a frequency domain analysis of commanded and measured signals, such as *Adaptive Phase-lead Compensator* [8] or *Windowed FEI Compensation* [9]. Other methods like *Adaptive Time Series* [10] and *Conditional Adaptive Time Series* [11] estimate the plant through Taylor series expansion and adjust the parameters in the time domain. *Adaptive model-based compensation* [12] consists of an estimate of the plant in frequency-domain; then, compensation is implemented in time-domain using numeric derivatives of the commanded signal and adaptation based on gradient. Some methods use polynomial extrapolation, such as the *Adaptive Two-Stage Compensation* [13] or the *Improved Adaptive Forward Prediction* [14]. Usually, adaptive methods have proved to be very efficient when there is uncertainty or non-linearity in the control plant; however, they are highly dependent on prior knowledge of the system to establish initial conditions and constraints for the adaptive parameters. Therefore, it is generally required to test the control plant with the experimental substructure included in order to perform the design and calibration of the controller. This methodology can cause premature damage to the physical specimen to be tested.

The objective of this study is to develop an adaptive compensator which is independent of the experimental substructure to be tested, avoiding the premature testing of the physical specimen. The *Adaptive Model-based Compensation* [12] method is used with the following modifications: (i) first-order controller; (ii) modified filter for the adaptation process; (iii) initial parameters based on a model of the transfer system without interaction with the experimental substructure; (iv) adaptive gains calibration through off-line numerical simulations using particle swarm optimization. The method is implemented in a virtual *RTHS* benchmark problem developed by Silva et al. [15]. This paper has the following organization. Section 2 describes the *RTHS* benchmark problem, the simulation cases, and the evaluation criteria to assess its

performance. Section 3 presents the proposed compensation method, with the formulation of the optimal adaptive gain calibration process. Section 4 presents the main results of the simulations for different partitioning cases in order to study the robustness of the proposed compensator. Lastly, Section 5 presents the conclusions and final remarks.

2. Problem formulation

2.1 RTHS benchmark problem

The *RTHS* benchmark problem [15] consists of a three-story moment frame with three lateral degrees of freedom, as shown on the left side of Fig. 1. The reference structure is divided into a numerical substructure (NS) and an experimental substructure (ES), as shown on the right side of Fig. 1.

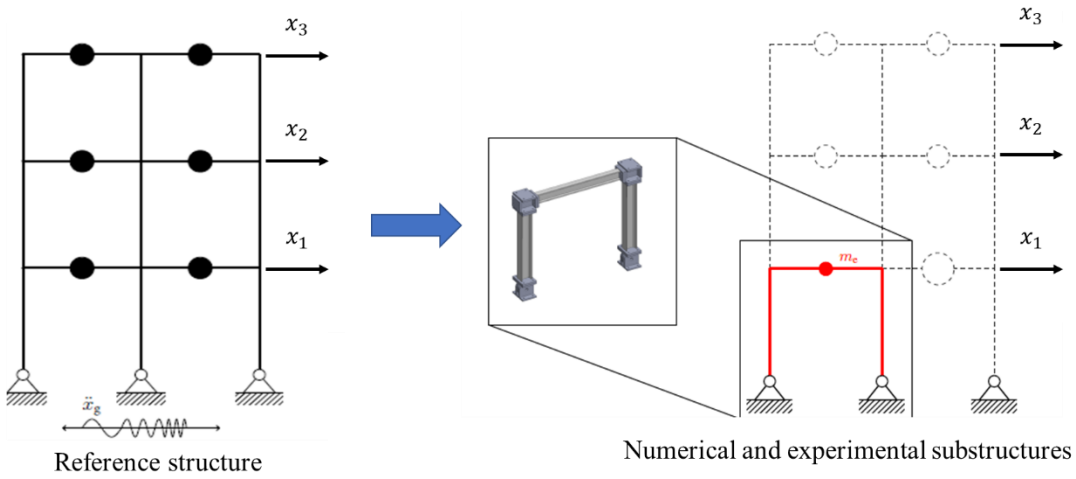

Fig. 1 – Reference structure and partitioning. Adapted from [15]. (Note: NS = dashed line; ES = red line.)

The equation of motion of the linear reference structure is presented in Eq (1).

$$M_r\ddot{x} + C_r\dot{x} + K_r x = -M_r\, r\, \ddot{u}_g \tag{1}$$

where M_r, K_r, and C_r are the mass, stiffness and damping matrices, respectively. x, $\dot{x}$, and $\ddot{x}$ are the displacement, velocity, and accelerations vectors, respectively, all measured relative to the ground motion. $\ddot{u}_g$ is the ground acceleration, and r is the seismic influence vector, taken as $r = [1\ 1\ 1]^{\mathrm{T}}$ for this problem.

The equation of motion of the numerical substructure (NS) is presented in Eq (2).

$$M_n\ddot{x}_n + C_n\dot{x}_n + K_n x_n = -M_r\, r\, \ddot{u}_g - [1\ 0\ 0]^T f_e \tag{2}$$

where subscript n refers to numerical substructure (NS). Subsequently, f_e is the measured restoring force from the experimental substructure (ES) described in Eq (3).

$$f_e = m_e\ddot{x}_m + c_e\dot{x}_m + k_e x_m \tag{3}$$

where m_e, k_e, and c_e the mass, stiffness, and damping parameters of the experimental substructure. In *RTHS*, the displacement of the first DOF from NS, $x_{n,1}$, is considered the target displacement x_t. Meanwhile, x_m corresponds to the measured displacement of ES and in the ideal case $x_m = x_{n,1}$, which satisfies compatibility in the boundary between substructures.

The block diagram utilized to solve this problem is presented in Fig. 2, which was implemented in Matlab and Simulink. For direct numerical integration, a 4th Order Runge-Kutta solver with a fixed time step

$\Delta t = 1/4096$ [sec] was considered. The output signal from the dynamic compensator is called command displacement and is denoted with the variable x_c. Noise has been added to measured signals to simulate physical sensors. Also, the output of the reference structure is the displacement of the first floor and is denoted as x_r. This signal is utilized to compare with the results of the *RTHS* to assess its accuracy.

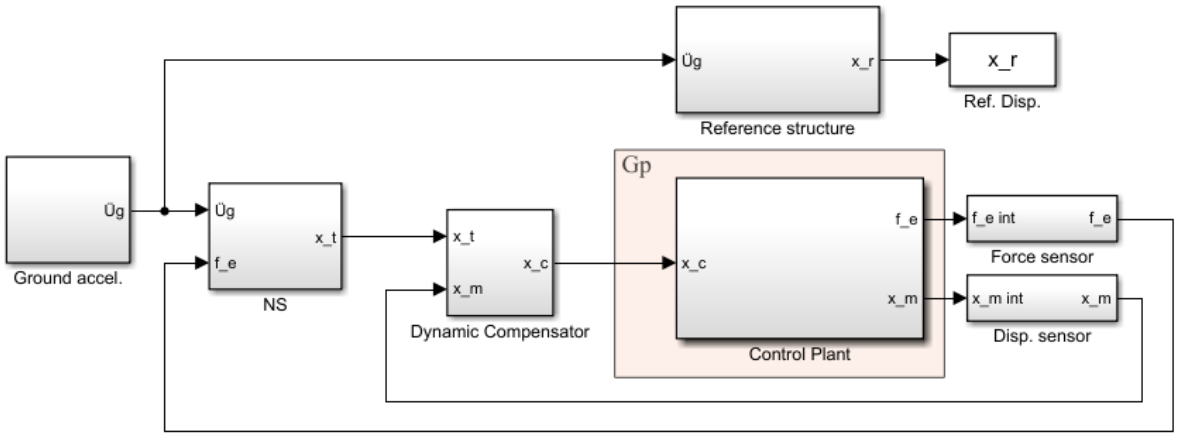

Fig. 2 – Simulink model for reference structure and *RTHS* closed-loop model.

The control plant (i.e., the actuator connected to ES) is modeled as shown in Fig. 3, where s corresponds to the Laplace variable, $s = j\omega$; j is the complex number, and ω is the circular frequency in [rad/s]. The parameters of the transfer system model are listed in Table 1, including uncertainties in three parameters represented by normally distributed and mutually independent random variables.

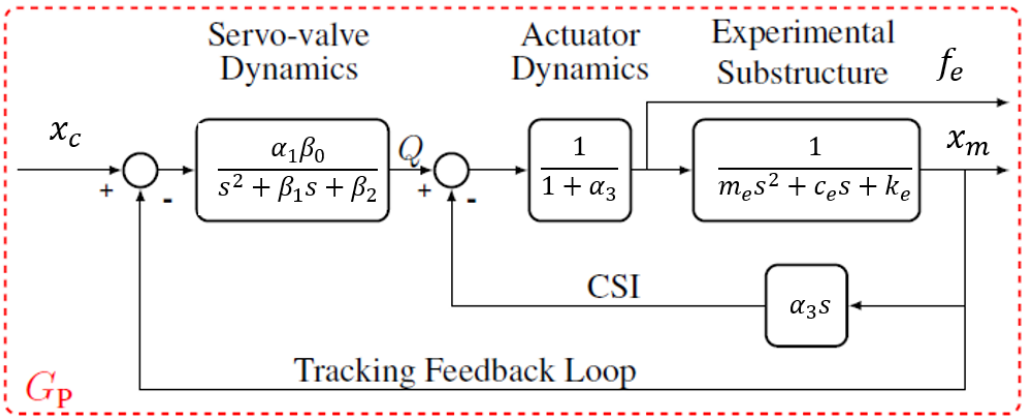

Fig. 3 – Control plant model. Adapted from [15].

Table 1 – Transfer system parameters.

Parameter	Nominal Value	Standard Deviation	Units
$\alpha_1\beta_0$	2.13×10^{13}	–	m-Pa/sec
α_2	4.23×10^{6}	–	m-Pa
α_3	3.3	1.3	1/sec
β_1	425	3.3	Nondimensional
β_2	1×10^{5}	3.31×10^{3}	1/sec

2.2 Simulation cases

The benchmark problem proposes different partitioning cases consisting of different mass and damping for the reference structure, resulting in different numerical substructure but the same experimental substructure for each case. In this paper, four cases are presented to evaluate the performance of the proposed control method, including uncertainties in the stiffness represented by a normally distributed random variable. The values for each case are listed in Table 2. Case I correspond to the most sensitive case from the benchmark problem, while Case II corresponds to the less sensitive. Case III and IV include different experimental substructures. For each case, the reference structure has the same mass per floor and the same damping for all modes.

Table 2 – Properties of simulation cases.

Case	Earthquake	Reference Structure			Numerical Substructure			
		Mass [kg]	**Frequencies [Hz]**	**Damping [%]**	m_e **[kg]**	c_e **[kg/sec]**	k_e **(mean)** $[\times 10^6$**N/m]**	k_e **(std.)** $[\times 10^4$**N/m]**
I	El Centro 40%	1000	3.6 ; 16.0 ; 38.1	3	29.1	114.6	1.19	5
II	Kobe 40%	1000	3.6 ; 16.0 ; 38.1	5	29.1	114.6	1.19	5
III	Kobe 40%	1100	3.1 ; 13.5 ; 32.2	3	40	200	1.79	10
IV	El Centro 50%	800	4.0 ; 17.9 ; 42.6	5	20	100	0.82	8

2.3 Evaluation criteria

The results are evaluated through three performance indicators:

- J_2: Normalized root-mean-square error between the target displacement x_t and the measured displacement x_m (Eq (4)). Measure the synchronization error.

$$J_2 = \sqrt{\frac{\sum_{l=1}^{L}(x_m[l] - x_t[l])^2}{\sum_{l=1}^{L}(x_t[l])^2}} \times 100\% \tag{4}$$

- τ: Corresponds to the delay indicator obtained with the frequency evaluation index [16]. Measure the synchronization delay (in milliseconds) between x_t and x_m.
- J_4: Normalized root-mean-square error between the reference displacement x_r and the measured displacement x_m (Eq (5)). Measure the error between the simulation and the reference structure.

$$J_4 = \sqrt{\frac{\sum_{l=1}^{L}(x_m[l] - x_r[l])^2}{\sum_{l=1}^{L}(x_r[l])^2}} \times 100\% \tag{5}$$

3. Methodology

3.1 Adaptive model-based compensation

The control method presented in this paper is based on the *Adaptive Model-based Compensation* (*AMBC*) [12]. The original method consists of a third-order adaptive feedforward combined with an LQG feedback regulator. In this study, a first-order adaptive controller is presented to show the calibration process in detail. The LQG is not considered for two reasons: (i) to demonstrate the compensation capacity of the adaptive feedforward; and (ii) the LQG method requires good knowledge to design the controller.

The formulation consists of estimating the plant by a first-order transfer function without zeros, as shown in Eq (6).

$$x_m \approx G_p(s)\, x_c = \frac{1}{a_1 s + a_0} x_c \tag{6}$$

Then, the inverse of this transfer function is used to generate the command signal using the target displacement as input, as shown in Eq (7).

$$x_c = G_p^{-1} x_t = (a_1 s + a_0) x_t = a_1 \dot{x}_t + a_0 x_t \tag{7}$$

The parameters a_0 and a_1 must be adjusted during the test to achieve good compensation. Therefore, Eq (6) is reordered to obtain a relation between the commanded and measured displacements, as shown in Eq (8).

$$x_c = [\, a_1 \; a_0][\, s\, x_m \quad x_m]^T = a_1 \dot{x}_m + a_0 x_m \tag{8}$$

In the original *AMBC* method, a low-pass filter $1/(1+s)^3$ is used to make proper transfer functions to obtain the derivatives of x_m. This filter affects the amplitude of the measured signal deteriorating the adaptation process. In this paper, a Butterworth filter is utilized to remove high-frequency noise and then calculate a numeric derivative to obtain $\dot{x}_m$, just like in other methods such as *Adaptive Time Series* [10] and *Conditional Adaptive Time Series* [11]. The filter is applied to the commanded signal to synchronize with the filtered measured signal. Once obtained the derivatives of x_m, an estimation error ε could be obtained, as shown in Eq (9).

$$\varepsilon = \frac{z - \hat{z}}{m_s^2} = \frac{z - \hat{\theta}^T w}{m_s^2} \tag{9}$$

where z is the filtered commanded signal x_c, $\hat{z}$ is the estimate of z, $\hat{\theta}$ is a vector that contains $\hat{\theta} = [a_0 \; a_1]^T$, and w is the filtered measured signal $w = [x_m \; \dot{x}_m]^T$. m_s^2 is the normalizing signal $m_s^2 = 1 + \alpha w^T w$; with $\alpha = 1$ in this paper. Once the estimated error is formulated, a cost function is defined in Eq (10).

$$J(\theta) = \frac{\left(z - \hat{\theta}^T w\right)^2}{2\, m_s^2} \tag{10}$$

Finally, using the adaptive gradient law, the rate of change is obtained, as shown in Eq (11).

$$\dot{\hat{\theta}} = \Gamma \varepsilon w \tag{11}$$

where Γ is the adaptive gain matrix. In this paper, Γ is assumed to be a diagonal matrix, where $\Gamma = \mathrm{diag}(\Gamma_0, \Gamma_1)$. These adaptive gains are related to the rate of adaptation parameters, and its calibration is discussed in Section 3.3.

Additionally, the original *AMBC* method considered the Routh's stability criterion to provide constraints for the adaptive parameters a_i. In this study, Routh's stability criterion is considered insufficient because it is based on the stability of the control plant being estimated, which does not guarantee the stability of the *RTHS* close-loop system. Thus, the stability of a compensation method in *RTHS* still a pending issue.

3.2 Specimen interaction in RTHS testing

Due to control-structure interaction [3], the transfer function of the plant will change every time the experimental substructure is changed, so in many control methods, the controller must be redesigned for each particular case. In this paper, the controller is designed to be used with different experimental substructures, avoiding system identification tests for each substructure to be tested.

The initial parameters a_0 and a_1 are defined with an estimation of the transfer system without interaction with any experimental substructure. In this paper, the parameters a_0 and a_1 are only restricted to $a_0 > 0$ and $a_1 > 0$, allowing free adaptation. The filter utilized in adaptation law is a fourth-order Butterworth

filter with a cutoff frequency of 20 [Hz]. In Fig. 4 the transfer function associated with initial parameters a_0 and a_1 are presented.

For the calibration process, a model of the transfer system connected to a calibration structure is utilized. This structure must show considerable interaction with the transfer system, and it is used only to obtain a calibration plant model from a commanded displacement to a measured displacement. In this paper, a calibration structure different to the experimental substructures used in *RTHS* is utilized, whose properties are $m_e = 60$ [kg], $k_e = 4 \times 10^6$ [N/m] and $c_e = 310$ [kg/sec]. The transfer functions of the calibration plant and the plant for each *RTHS* case with nominal values are presented in Fig. 4. The transfer functions are presented from 0 [Hz] to 100 [Hz], but the most significant frequencies in seismic testing are approximately 0-20 [Hz]. Cases I and II have the same experimental substructure, so present the same transfer function, while Case III and Case IV exhibit different transfer functions due to the different experimental substructures. All the plants have different behavior with respect to the initially estimated plant, showing different levels of interaction with the transfer system. Thus, the parameters a_0 and a_1 must be adjusted to achieve good compensation.

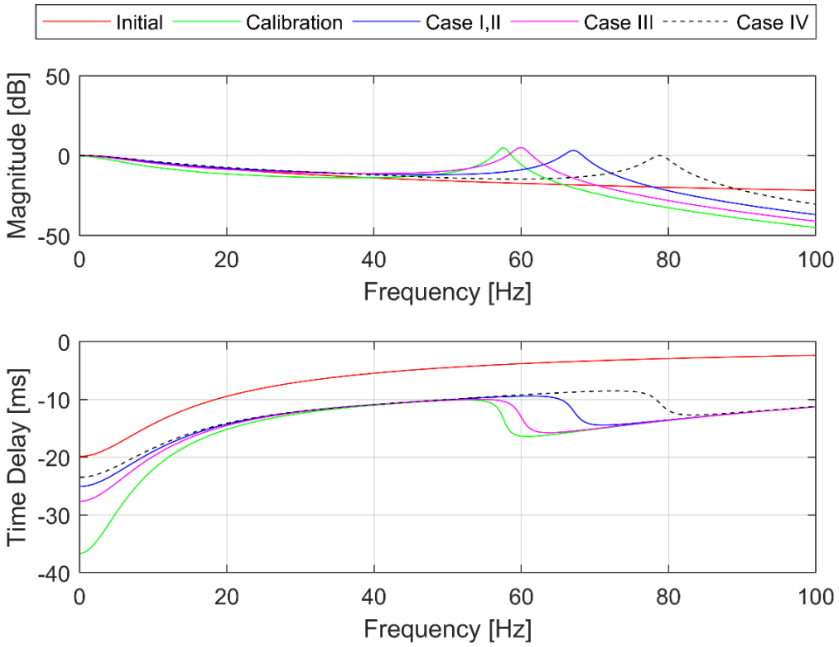

Fig. 4 – Bode diagrams of transfer function $G_P(s)$

3.3 Optimal calibration of adaptive gains

For the calibration, a Simulink model is utilized to evaluate different off-line pairs of Γ_0 and Γ_1. The Simulink model is presented in Fig. 5 and consists in: (i) ground acceleration (in this calibration, El Centro earthquake scaled to 60%); (ii) a calibration structure to generate a target displacement (in this calibration, a single degree of freedom structure with natural frequency of 5 [Hz] and 5% damping ratio); (iii) the adaptive controller with initial conditions according to red curve Fig. 4 and predefined adaptive gains Γ_0 and Γ_1; (iv) calibration plant model (green curve of Fig. 4); and (v) noise addition to the measured displacement to model the sensor.

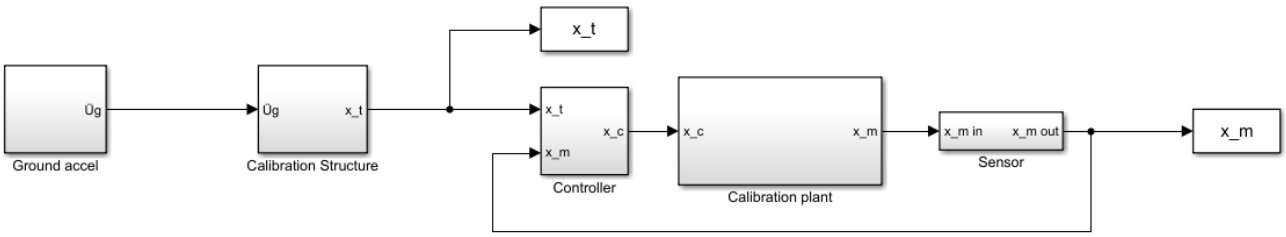

Fig. 5 – Simulink model for calibration.

The J_2 indicator is selected to evaluate the controller performance because it represents the tracking error, and minimizing this error, stable and accurate results are expected. So, for each simulation, the J_2 indicator is computed to measure the error between the target and measured displacement. Thus, the calibration consists of obtaining the adaptive gains, which minimizes the J_2 performance indicator. This study proposes particle swarm optimization to find the optimal adaptive gains, but other optimization methods could be used as well. Particle swarm optimization [17] consists of defining several particles (N), where the position of each particle represents a possible solution to minimize a fitness function. In this calibration, $x_i[k]$ represents the position $[a, b]$ for the particle $i \in [1, N]$ at the iteration $k \in [1, K]$, where K is the total number of iterations. The position is related to the adaptive gains such that $\Gamma = \text{diag}(\Gamma_0, \Gamma_1) = \text{diag}(10^a, 10^b)$. Thus, for each position, there is an error indicator $J_2(x_i[k])$ resulting from the simulation with the adaptive gains associated with position $x_i[k]$. Next, a set of n particles with random initial positions and velocities are defined in a constrained search space. Then, the position and velocity of each particle are updated, according to Eq (12) and Eq (13).

$$v_i[k+1] = \omega v_i[k] + r_1[k]c_1(p_i[k] - x_i[k]) + r_2[k]c_2(g[k] - x_i[k]) \quad (12)$$

$$x_i[k+1] = x_i[k] + v_i[k+1] \quad (13)$$

where $v_i[k]$ is the velocity of particle i at iteration k. The velocity is updated according to a weighted sum of three components: (i) inertia with weight ω; (ii) difference between the position with best result of the particle $p_i[k]$ and the current position $x_i[k]$, with a random component $r_1[k]$ and weight c_1; and (iii) the difference between the position with best result of the swarm $g[k]$ and the current position $x_i[k]$, with a random component $r_2[k]$ and weight c_2. The best position of a particle $p_i[k]$ corresponds to the position with the lowest J_2 value for the particle i. Whereas, the best position of the swarm $g[k]$ corresponds to the position with the lowest J_2 value for all particles.

In this calibration, the lower and upper bounds are set to $x_i^{\text{lower}} = [4,3]$ and $x_i^{\text{upper}} = [7,6]$, resulting in $\Gamma_0 \in [10^4, 10^7]$ and $\Gamma_1 \in [10^3, 10^6]$. The results of the optimization method in terms of J_2 value for a pair $[\Gamma_0, \Gamma_1]$ are presented in Fig. 6 with a few iterations and particles ($K = 5$ and $N = 5$; i.e., 25 simulations) where each marker represents a particle and each color a different iteration. The contour map was obtained from sampling with a uniform grid of 400 simulations. The contour levels show that many combinations of $[\Gamma_0, \Gamma_1]$ result in good tracking ($J_2 < 10\%$), while other combinations with higher values of Γ_1 results in bad tracking performance ($J_2 > 80\%$). Also, after analyzing the optimization process in Fig. 6, it can be noticed that the particles move from their initial random position to the global optimal. Finally, the best result of the swarm is indicated by the blue circle.

The adaptive gains obtained with different numbers of particles and iterations are presented in Table 3. Finally, the best results are $\Gamma_0 = 2.38 \times 10^6$ and $\Gamma_1 = 1.10 \times 10^5$. These adaptive gains are utilized for the *RTHS* simulations, whose results are presented in Section 4.

Table 3 – Optimization results.

Optimization	**No. Particles** N	**No. Iterations** K	$\boldsymbol{\Gamma_0^*}$ $[\times 10^6]$	$\boldsymbol{\Gamma_1^*}$ $[\times 10^5]$	$\boldsymbol{J_2^*}$ [%]
1	5	5	2.36	1.29	5.369
2	10	5	2.87	1.92	5.383
3	5	10	2.57	1.46	5.370
4	10	10	2.38	1.10	5.367

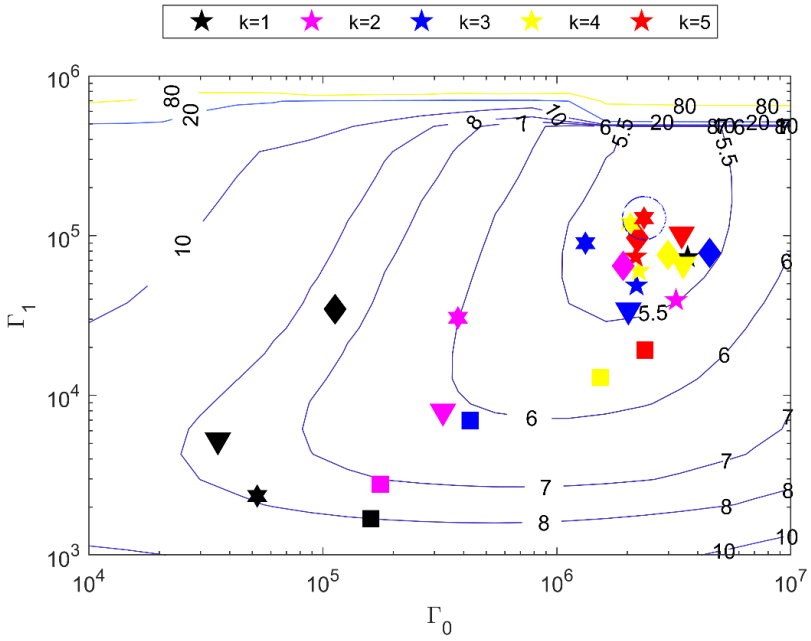

Fig. 6 – Particle swarm optimization for adaptive gains (Note: color = iteration; marker = particle).

4. Results

4.1 RTHS Case I

The results of *RTHS* Case I with nominal values and using $\Gamma_0 = 2.38 \times 10^6$and $\Gamma_1 = 1.10 \times 10^5$ are presented graphically in this subsection. In Fig. 7, the measured displacement is compared with the target displacement for tracking evaluation. With $J_2 = 2.58$ [%] and $\tau = 0.033$ [msec], good tracking is achieved, allowing a stable test. Meanwhile, Fig. 8 shows a comparison between the measured displacement and the reference displacement. The J_4 indicator reaches only 3.21%, which means accurate results were obtained.

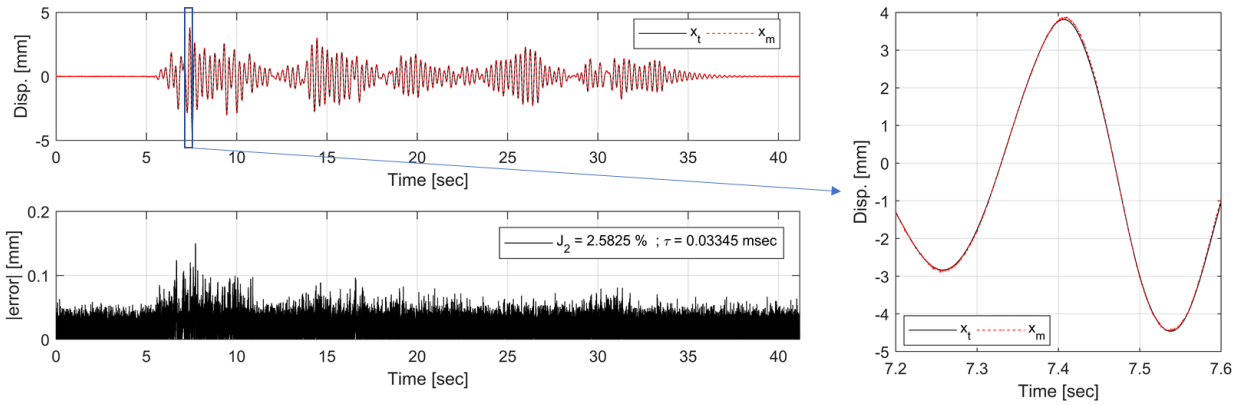

Fig. 7 – Target and measured displacements results for Case I.

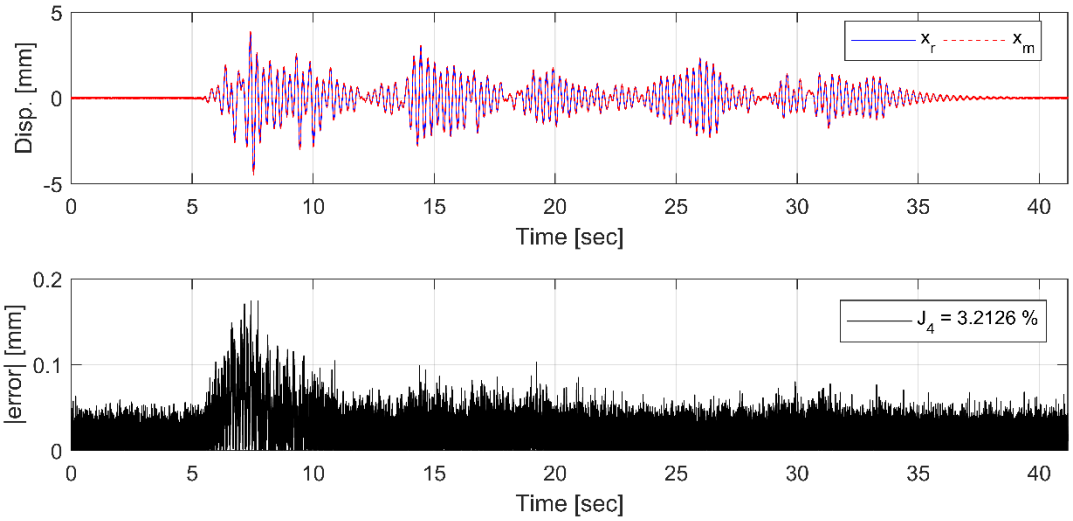

Fig. 8 – Reference and measured displacements results for Case I.

Parameter adaptation during the test is presented in Fig. 9, where it can be noted that the parameters show more adaptation at the beginning of the earthquake (i.e., after 5 [sec]), which demonstrates fast adaptation. The parameters show convergence during the earthquake, allowing to estimate the plant and achieving reasonable compensation. The adaptation process for Case I is contrasted with adaptation for the other cases. The initial parameters are the same for all cases but converge to different values due to the differences in the control plant. The parameter a_0 is related to the amplitude errors of the control plant. Since both Cases I and II are subjected to different excitations, the response of the plant in each case presents different amplitude errors. Thus, parameter a_0 converges in each case to slightly different values. Meanwhile, the parameter a_1 is directly related with the time delay of the control plant and can be observed that this parameter for both Cases I and II converge to the same value, while Case III converge to higher value of a_1 and Case IV to a lower a_1, which is consistent with time delays presented in Fig. 4. Notice that parameters a_0 and a_1 try to identify the control plant through a first-order transfer function. However, the real system has a more complex behavior, so the estimated parameters may vary depending on the commanded displacements.

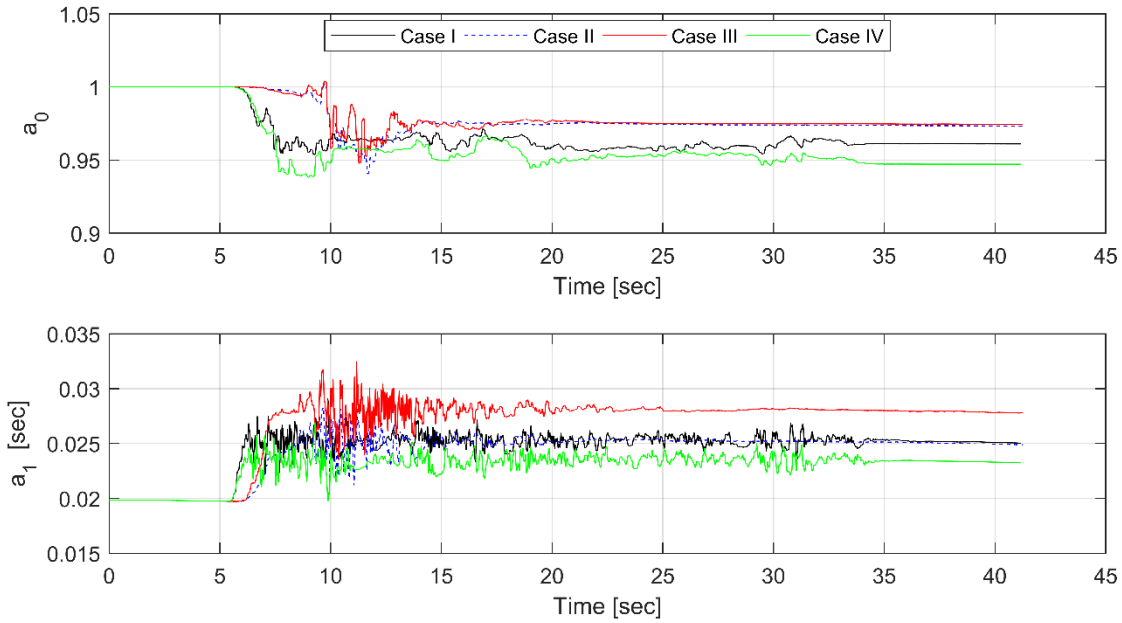

Fig. 9 – Parameter adaptation during the test for all cases.

4.2 Robustness of the proposed method

The statistics for 20 simulations for each case are presented in Fig. 10, where the red line corresponds to the median, and the bottom and top limits indicate the 25th and 75th percentile, respectively. The whiskers extend to the most extreme values. Outliers (if present) are represented by '+' symbol. Notice that the same controller allows excellent compensation for all different cases. This adaptation capacity allows not only to control different plants, but it also shows excellent robustness against uncertainties and noise. It could also maintain a suitable performance if the experimental substructure changes its properties considerably during the test.

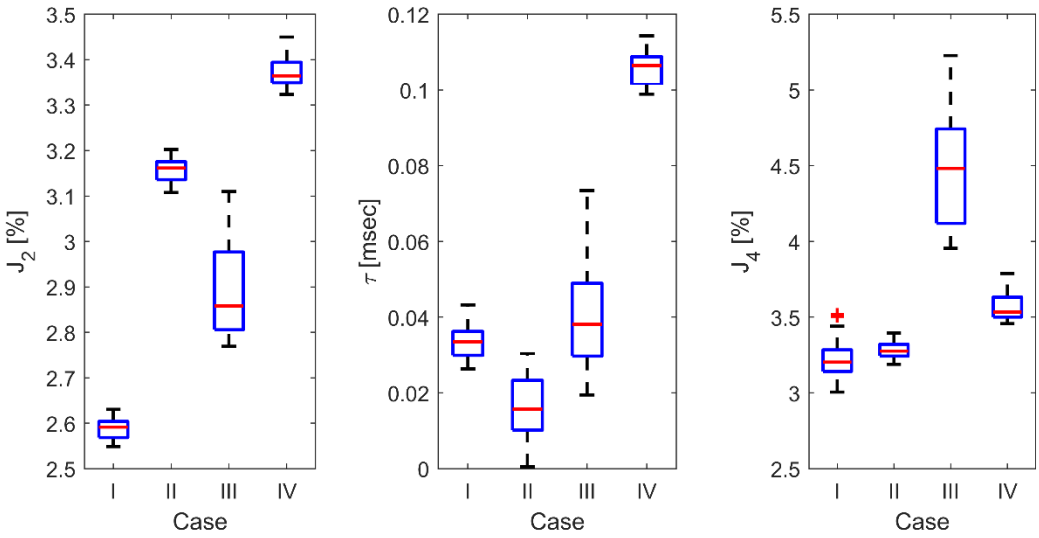

Fig. 10 –*RTHS* performance with the proposed compensation method. (Note: 20 simulations per case.)

5. Conclusions

This study presents the design and calibration process of an adaptive controller for real-time hybrid simulation. Initial parameters are based only on the transfer system without specimen interaction, and adaptive model-based compensation is utilized to adjust control parameters during the test to capture the interaction above. The adaptive gains of the controller are adjusted through "off-line" numerical simulations using particle swarm optimization, which allows finding optimal gains with a reasonable number of iterations. After gain calibration, a virtual *RTHS* experiment with different control plants was conducted, including uncertainties in the transfer system and experimental substructure properties. The results demonstrate that a fixed robust controller could be used with different experimental substructures, avoiding subsequent system identification tests. Even though this study considered only linear systems for the numerical and experimental substructures, it is expected that it also works with non-linear systems since the controller can adapt to different control plants. The first-order control method presented in this paper could also be extended for a higher-order controller using the same optimization process for the calibration, allowing to represent more complex control plants. Finally, this adaptive method should be complemented with a stability analysis during the *RTHS* before its application in the laboratory.

6. Acknowledgments

The authors gratefully acknowledge the financial support from the Universidad Técnica Federico Santa Maria (Chile) through the research grant *Proyecto Interno de Línea de Investigación* No. PI_L_18_07, and from the Chilean National Commission for Scientific and Technological Research (CONICYT), FONDECYT-Iniciación research project No. 11190774. Any opinions, findings, conclusions, or recommendations expressed in this paper are those of the authors and do not necessarily reflect those of the sponsors.

7. References

[1] M. Nakashima, H. Kato, and E. Takaoka, "Development of real-time pseudo dynamic testing.," *Earthq. Eng. Struct. Dyn.*, vol. 21(1), pp. 79–92, 1992.

[2] D. P. McCrum and M. S. Williams, "An overview of seismic hybrid testing of engineering structures," *Eng. Struct.*, vol. 118, pp. 240–261, Jul. 2016.

[3] S. J. Dyke, B. F. Spencer, P. Quast, and M. K. Sain, "Role of control-structure interaction in protective system design," *J. Eng. Mech.*, vol. 121, no. 2, pp. 322–338, 1995.

[4] A. Maghareh, S. Dyke, S. Rabieniaharatbar, and A. Prakash, "Predictive stability indicator: a novel approach to configuring a real-time hybrid simulation," *Earthq. Eng. Struct. Dyn.*, vol. 46, no. 1, pp. 95–116, 2017.

[5] T. Horiuchi, M. Inoue, T. Konno, and Y. Namita, "Real-time hybrid experimental system with actuator delay compensation and its application to a piping system with energy absorber," *Earthq. Eng. Struct. Dyn.*, vol. 28, no. 10, pp. 1121–1141, 1999.

[6] C. Chen and J. M. Ricles, "Tracking Error-Based Servohydraulic Actuator Adaptive Compensation for Real-Time Hybrid Simulation," *J. Struct. Eng.*, vol. 136, no. 4, pp. 432–440, Apr. 2010.

[7] J. E. Carrion and B. F. Spencer, "Model-based Strategies for Real-time Hybrid Testing," *Newmark Struct. Eng. Lab. Rep. Ser. 006, Univ. Illinois Urbana-Champaign.*, 2007.

[8] J. Tao and O. Mercan, "A study on a benchmark control problem for real-time hybrid simulation with a tracking error-based adaptive compensator combined with a supplementary proportional-integral- derivative controller," *Mech. Syst. Signal Process.*, vol. 134, p. 106346, 2019.

[9] W. Xu, C. Chen, T. Guo, and M. Chen, "Evaluation of frequency evaluation index based compensation for benchmark study in real-time hybrid simulation," *Mech. Syst. Signal Process.*, vol. 130, pp. 649–663, 2019.

[10] Y. Chae, K. Kazemibidokhti, and J. M. Ricles, "Adaptive time series compensator for delay compensation of servo-hydraulic actuator systems for real-time hybrid simulation," *Earthq. Eng. Struct. Dyn.*, vol. 42, no. 11, pp. 1697–1715, Sep. 2013.

[11] A. Palacio-Betancur and M. Gutierrez Soto, "Adaptive tracking control for real-time hybrid simulation of structures subjected to seismic loading," *Mech. Syst. Signal Process.*, vol. 134, p. 106345, 2019.

[12] P.-C. Chen, C.-M. Chang, B. F. Spencer, and K.-C. Tsai, "Adaptive model-based tracking control for real-time hybrid simulation," *Bull. Earthq. Eng.*, vol. 13, no. 6, pp. 1633–1653, Jun. 2015.

[13] Z. Wang, X. Ning, G. Xu, H. Zhou, and B. Wu, "High performance compensation using an adaptive strategy for real-time hybrid simulation," *Mech. Syst. Signal Process.*, vol. 133, p. 106262, 2019.

[14] D. Xu, H. Zhou, X. Shao, and T. Wang, "Performance study of sliding mode controller with improved adaptive polynomial-based forward prediction," *Mech. Syst. Signal Process.*, vol. 133, p. 106263, 2019.

[15] C. E. Silva, D. Gomez, A. Maghareh, S. J. Dyke, and B. F. Spencer, "Benchmark control problem for real-time hybrid simulation," *Mech. Syst. Signal Process.*, vol. 135, p. 106381, 2020.

[16] T. Guo, C. Chen, W. Xu, and F. Sanchez, "A frequency response analysis approach for quantitative assessment of actuator tracking for real-time hybrid simulation," *Smart Mater. Struct.*, vol. 23, no. 4, p. 045042, Apr. 2014.

[17] J. Kennedy and R. Eberhart, "Particle Swarm Optimization," in *Proceedings of the IEEE International Conference on Neural Networks. Perth, Australia*, 1995, pp. 1942–1945.

